



Impact of Weak Organic Acids as Coagulants on Tailoring the Properties of Cellulose Aerogel Beads

Diogo Costa,^[a, b] Barbara Milow,^[a, b] and Kathirvel Ganesan^{*[a]}

Tailoring the properties of cellulose aerogel beads was investigated in the present study by using weak organic acids as coagulants. Three different weak acids were specifically chosen, acetic acid, lactic acid and citric acid. For comparative studies, a strong acid, hydrochloric acid was examined. The production of aerogel beads by conventional dropping technique was controlled and optimized for weak acids. Aerogels were characterized by density analyses, scanning electron microscopy, nitrogen adsorption–desorption analysis, X-ray powder diffraction and IR spectroscopy. In common, all the aerogel beads showed interconnected nanofibrillar network, high specific surface area, high pore volume, high porosity and meso- and

macroporous structure. In particular, when the weakest acid (acetic acid) was used as coagulant in the regeneration bath, the lowest shrinkage was observed. As a result, the cellulose aerogel beads produced from acetic acid showed the highest values of specific surface area ($423 \text{ m}^2 \text{ g}^{-1}$) and pore volume ($3.6 \text{ cm}^3 \text{ g}^{-1}$). The porous structure can be tuned by the choice of regeneration bath, which has either strong acid or a high concentration of weak acid. The aerogel beads were pure and showed cellulose II crystallinity. Hence this study paves an alternative path way to tailor the properties of cellulose aerogel beads.

Introduction

The term “aerogel” was first coined by Kistler in 1931 and describes a solid gel where the liquid media was replaced by air, with minor shrinkage of the solid porous network.^[1] Aerogels possess open porous microstructure, high porosity, high specific surface area and low-density. Interest in developing bio-based aerogels has been exponentially growing in various fields since 2000.^[2] Aerogels of polysaccharides, especially cellulose-based porous materials, receive great attention in many applications including thermal insulators,^[3] oil-adsorbents^[4] and in bio-medicine.^[5] This is due to the fact that they are produced from renewable resources and exhibit no toxicity, high biocompatibility and biodegradability. Similar to other polysaccharide aerogels, cellulose aerogels consist of interconnected nanofibrillar networks.

Distinct from crystalline cellulose I aerogels, regenerated cellulose aerogels exhibit a thermodynamically stable crystalline structure, cellulose II. Regenerated cellulose aerogel beads are prepared in general by dissolution, gelation, solvent exchange and drying. The results of comprehensive studies in the literature demonstrate that the physical and structural proper-

ties of regenerated cellulose aerogels have been remarkably influenced by dissolution and gelation (regeneration).^[6] Other factors such as the solvent exchange and the drying process can also influence the aerogel properties but the impact occur only on the existing hydrogel network.^[6,7]

Cellulose solvents such as aqueous alkali medium (optionally with additives), ionic liquids and molten salt hydrates are frequently used for the production of regenerated cellulose aerogels.^[6b,8] Depending on the conditions for the dissolution of cellulose, the physical interactions between cellulose molecules can vary in accordance with the chemical and physical environment of the cellulose chains in solution. In a preparation process of regenerated cellulose aerogels, after dissolution, the cellulose molecules are sensitive to their physical and chemical environment. They tend to aggregate into interconnected nanostructures. During gelation, the aggregation behaviour of cellulose can undergo distinctive path ways which differ from each other under various controlled conditions such as temperature, pH, aging and diffusion of nonsolvent. This leads to remarkable differences in morphology depending upon the respective cellulose-solvent medium. For instance, it was demonstrated in the literature^[9] that aerogels prepared from different cellulose solvents such as NaOH-water, NMMO, EMIMAc and BMIMAc exhibited diverse physical properties including the bulk density, specific surface area, morphology and mechanical strength.

The regeneration bath should be a cellulose non-solvent and it can vary in polarity, pH and ionic strength, e.g., organic solvents (ethanol, acetone, iso-propanol), water, acidic medium (H_2SO_4 , HCl , HNO_3) and salt solutions (NaCl , CH_3COONa , Na_2SO_4 , $(\text{NH}_4)_2\text{SO}_4$).^[9,10] The regenerated cellulose aerogel beads were mostly prepared from NaOH-water mixture. Zhang et al.^[10b] explored the effect of coagulation conditions of acetic acid on the properties of regenerated cellulose films. With weak

[a] D. Costa, B. Milow, K. Ganesan
German Aerospace Center (DLR), Institute of Materials Research, Linder
Hoehe, 51147 Cologne, Germany
E-mail: k.ganesan@dlr.de

[b] D. Costa, B. Milow
University of Cologne (UoC), Department of Chemistry, Nanostructured
Cellular Materials, Greinstraße 6, 50939 Cologne, Germany

© 2024 The Authors. Chemistry - A European Journal published by Wiley-VCH GmbH. This is an open access article under the terms of the Creative Commons Attribution Non-Commercial License, which permits use, distribution and reproduction in any medium, provided the original work is properly cited and is not used for commercial purposes.

dissociation of acetic acid at the reaction front, the coagulation process resulted in producing aerogel with densely packed nanofibrillar networks and high mechanical properties. Further studies were carried out by Zhang et al.^[10b] with a series of other coagulants such as H_2SO_4 , $\text{H}_2\text{SO}_4/\text{Na}_2\text{SO}_4$, Na_2SO_4 and $(\text{NH}_4)_2\text{SO}_4$. It was reported that the composition and concentration of coagulant systems and the temperature set for regeneration bath can strongly influence the optical and mechanical properties of cellulose films. The authors^[10b] proposed that the coagulation mechanism in this NaOH-urea-water solvent medium was described as a two-phase separation process, namely a cellulose-rich phase forming gel network and a cellulose-poor phase in solution precipitating and regenerating the cellulose. Gavillon and Budtova^[9a] studied the kinetics of the cellulose regeneration for NaOH-water systems. It was found that the rheological activation and diffusion activation energies coincided for NaOH-water system. The results confirmed that the NaOH-water system is a suspension of hydrated ions of NaOH with or without cellulose. Hence, it was concluded that the independent movement of hydrated NaOH molecules played a vital role in the regeneration of cellulose leading to a phase separation process, producing a swollen cellulose in nonsolvent. It was described that the coagulation occurred by a diffusion-controlled movement of hydrated ions and nonsolvent molecules in cellulose-NaOH-water system.

The earliest study was reported in 1988 for the production of the regenerated cellulose particles.^[10a] In this study, the porous cellulose particles were regenerated from cellulose xanthate-NaOH-water mixture by acid (H_2SO_4) hydrolysis. Gavillon^[10c] prepared cellulose wet beads from cellulose-NaOH (8%)-water mixture by cutting the jet of liquid before entering the H_2SO_4 regeneration bath. Later, the wet beads were washed, solvent exchanged with acetone and dried under supercritical carbon dioxide. Cai et al.^[10d] produced cellulose aerogel films from the mixture of cellulose-alkali hydroxide (LiOH or NaOH)-urea-water by using aqueous solution of 5% H_2SO_4 as regeneration bath. In common, both the aqueous alkali hydroxide medium yielded cellulose aerogels having a high specific surface area and finely distributed porous structures. In the recent studies of Schroeter et al.,^[10i] it was demonstrated that the specific surface area values did not depend on both the concentration of H_2SO_4 (from 5 wt% to 35 wt%) in regeneration bath and the concentration of cellulose (from 4 wt% to 7 wt%). However, the shape of the particle was affected, i.e., non-spherical particles were produced when the concentration of H_2SO_4 was below 25 wt%. Isobe et al.^[10e] studied the properties of cellulose gels produced from LiOH-urea-water solutions using a regeneration bath of methanol, ethanol, acetone, 5 wt% of H_2SO_4 in water or 5 wt% of Na_2SO_4 in water. Nanofibrillar structures and membrane-like structures were produced for organic and aqueous coagulants respectively because the polarity of the coagulant induced different aggregation behavior of cellulose molecules and consequently tailored the morphology of the aerogels. Trygg et al.^[10f] showed the impact of the various concentrations of HNO_3 on the regeneration of cellulose in NaOH-urea-water system. It was concluded that a higher concentration of acid created an outer

cellulose shell, and the nucleation of the nano-network of cellulose occurred from the outer shell by the diffusion of ions. Whereas in the case of low concentration of acid, the regeneration process homogeneously occurred from the droplet surface to its interior. It influenced also the specific surface area values of aerogels. In one of our previous studies, the effect of addition of ZnO particles to the cellulose-NaOH-urea-water medium was explored.^[10g] Here, cellulose wet-gel beads were prepared (syringe dropping technique) by dropping the solution into an aqueous hydrochloric acid (HCl, 2 M) solution. It revealed that the addition of 0.5 wt% of ZnO particles as additive improved the physical and morphological properties of cellulose aerogel particles.

Thus, the tuning of the aerogel's properties can be achieved by selecting the regeneration bath through variation of cellulose nonsolvent and coagulation medium. Up to our knowledge, most acids used as regeneration bath are strong inorganic acids such as HCl, H_2SO_4 , HNO_3 and a mixture of their corresponding salts,^[10b,f,11] but not many publications focused on the utilization of organic molecules having carboxylic acid functional groups. In this current study, we evaluate the impact of different acids as regeneration baths in the production of cellulose aerogels beads: hydrochloric acid (HCl), acetic acid (HAc), lactic acid (HLac) and citric acid (HCit). This study helps us to improve the understanding of how different acids with different densities, strength and molecular structure, may influence the structural and physical properties (surface area, porosity, density, etc.,) of cellulose aerogel beads.

Results and Discussion

For the cellulose beads production, a conventional syringe dropping technique was utilized. A schematic diagram of a multi nozzle system is depicted in Figure 1a. Cellulose beads were prepared by dropping the cellulose solution in different regeneration bath containing organic or inorganic acids.

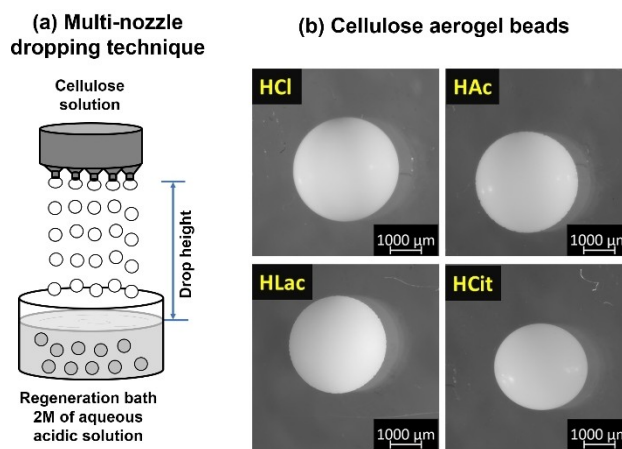


Figure 1. Schematic diagram of a conventional multi-nozzle dropping technique (a) and optical microscope images of cellulose aerogel beads produced from various acids in regeneration bath (b).

Considering the significance of pKa values, four different acids having various acid strengths were used as regeneration baths in this study. The organic acids were particularly interesting because of their weak acidity in comparison with HCl. The physical properties and chemical structure of acids are summarized in Table 1.

The droplets were produced by passing the viscous cellulose solution through the nozzles and letting them enter (under the gravitational force) into the regeneration bath. When the droplet of cellulose solution entered in the aqueous acidic solution, the regeneration of cellulose immediately occurred resulting in a thin film of cellulose network holding a liquid core of cellulose-NaOH-urea-water mixture. The continuous development of the randomly connected cellulose network happened inwards to the core by neutralizing the hydrated NaOH ions, decreasing the pH in the cellulose wet-gel body and diffusion of ions and molecules out from the wet-gel body until equilibrium. In this regeneration process, the beads shape was close to spherical.

The wet-gel body in the aqueous acidic medium was white in color after gelation. After washing and supercritical carbon dioxide drying (scCO₂) the aerogel samples were still white in color whereas after employing ambient drying, the sample turned to be glassy yellow in color. Example of aerogel beads obtained from different acid baths are shown in Figure 1b.

Optimizing the Conditions for Beads Production

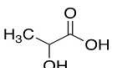
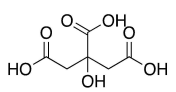
The drop height was kept constant by adjusting the distance between nozzle tip and surface of the rising level of the regeneration bath to maintain the spherical shape of the droplets and the beads after gelation because the volume of the regeneration bath was increased. The drop-height was influenced by the nozzle diameter and the liquid properties of both the cellulose solution and the regeneration bath such as viscosity, surface tension, density, etc.^[13] Trailing the experiments with the regeneration bath of HAC (2 M), an optimum spherical shape of beads for Cell6 and Cell7 was produced. The deformed bead shape was partly obtained for Cell5. Additionally, in this case, the drop heights were critical to maintaining

≤ 10 mm which can be the optimum drop-height for Cell5. Setting the drop-height value for Cell5 at 20 mm resulted in disc-like particles. For cell7, the optimum drop height can be 13 mm which was not yet convenient for a multi-nozzle system. In this case, the drop-height was raised to 20 mm and the Cell7-beads having close to spherical shape were produced. Hence, in the case of Cell7, when different acids were employed, setting the drop height at 20 mm was convenient to produce beads close to spherical shape.

A linear relation between the density of the regeneration bath and the drop height was observed when the density of the regeneration bath was increased either by varying concentration of acid or changing the type of acid. For instance, in the case of Cell7 when the HAC was used as coagulant, the drop height was maintained at 8, 13, 15 and 16 mm for the concentration levels of 1, 2, 3 and 4 M, respectively. Below 1 M of HAC, the deformed bead shape was obtained whereas the beads shape was close to spherical if the concentration of acetic acid was maintained ≥ 2 M. Here, it has to be considered that the concentration of NaOH used in cellulose solution was 0.175 mole. In order to neutralize NaOH in aqueous medium and to regenerate the cellulose nano-network, first by forming an outer shell and then inwards the droplet producing a stable wet-gel shape, an equivalent concentration of acid is required. In the case of the concentration of HAC below 0.08 mole, the droplet of cellulose NaOH-urea-water mixture was not stable due to the slow reaction resulting in the deformed particles (refer Figure 6a). In the present study, as a minimum concentration of 0.2 mole of organic acids was adequate at the reaction front for the stable shell formation and thereby cellulose beads can be produced in close to spherical shape. Thus, the concentration of aqueous acidic solution in regeneration bath was kept at 2 M for all of the experiments considering the reduced usage of chemicals and their environmental impact.

In the case of Cell7, the density of cellulose-NaOH-urea-water mixture was measured to be 1.1277 g cm⁻³ and the decrease in cellulose concentration did not show a major effect in density values. The density values of aqueous acidic solutions are summarized in Table 1. Once the cellulose droplet (Cell7) touches the surface of the acid bath, the mechanical stress

Table 1. Structure and physical properties of aqueous acidic solutions.

Name of acids (abbreviation)	Chemical structure	pKa ^[a]	Density (2 M of aqueous solution)/g cm ⁻³	Surface tension ^[b] /mN m ⁻¹
Hydrochloric acid (HCl)	H—Cl	−6.1	1.0315	66.37
Acetic acid (HAc)		4.76	1.0142	51.33
L(+)-Lactic acid (HLac)		3.83	1.0375	51.79
Citric acid (HCit)		3.13; 4.76; 6.40	1.1522	64.56

[a] The pKa values were obtained from the literature.^[12] [b] Surface tension of water was calculated to be 71.24 mN m⁻¹ at 23 °C.

existing on the droplet surface may damage its shape. This stress can be related to the elasticity of the cellulose droplet and it is directly proportional to the density of the cellulose droplet, the density of the regeneration bath, the drop height and the gravitational force. The density values of acids were observed to be lower than the density of cellulose-NaOH-urea-water mixture, except for HCit which has the highest density. Therefore, excluding for Cell7-HCit, the droplets were confirmed to have less mechanical impact while touching the regeneration bath. In the case of Cell7-HCit, the particles showed a very little deformation (see Figure 1).

HAc has the lowest density and the density values of acids increases in the following order: HLac, HCl and HCit. The larger the difference in the density between the cellulose-NaOH-urea-water mixture and the acidic regeneration bath, i.e., when the ratio between them was above the density value of the regeneration bath, the easier the particles could move to the bottom of the regeneration bath. Whereas, the smaller difference in the densities, i.e., when the ratio was equal to or below the density of the regeneration bath, the particles stayed below the liquid surface instead of moving into the regeneration bath. For instance, in the case of HAc, the particles freely moved down to the bottom of the regeneration bath whereas, in the case of HCit, the droplets immersed in the regeneration bath and stayed in contact with the liquid surface until complete gelation occurred and ionic equilibrium reached. Moreover, in this case, the drop height was directly proportional to the density of the acid bath. By increasing the density of the regeneration bath, the drop height should also be increased to achieve a good spherical shape of beads. In the present study, in order to understand the influence of the acids in regeneration bath, the drop-height was maintained to be constant for all the acids which may give an optimized size and shape of beads and that was set to be 20 mm.

Size and Shape Analyses of Cellulose Beads

Mean particle size was calculated from the cumulative percentage distribution curve, Q3 (see Table 2). The mean diameter of the wet-gel beads in the acid bath was increased in the order of the samples: Cell7-HCit, Cell7-HLac, Cell7-HAc and Cell7-HCl. The surface tension of acid bath was examined (see Table 1) and considered for the particles size analysis. The acid baths (2 M) had surface tension values below the surface tension of

water (71.24 mNm⁻¹) and HAc and HLac showed low surface tension compared to HCit and HCl.

Organic acids with a greater number of hydrogen-bond donor-acceptor properties (with functional groups such as -COOH and -OH groups) can show high surface tension in water. Therefore, the organic acids chosen in the present study can show differences in the surface tension as the chemical structure have various functional groups. Especially HCit with functional groups, three times -COOH and one -OH showed very high surface tension, close to the value of HCl.

During regeneration of beads in organic acids, the particles size varied and increased in the order of following acids: HCit, HLac and HAc. It reveals that the carboxylic functional groups of organic acids, by having high hydrogen-bond donor-acceptor properties, could have strongly influenced the wet-gel network formation from shell to complete gelation. Hence, the interaction of the acids with cellulose, in specific with cellulose-OH functional groups, was enhanced when the hydrogen-bond donor-acceptor behavior of acids increased. As a result, the HCit with its strong interaction to cellulose reduced the particles size to be the smallest.

In the case of HCl bath (hydrated ions of H⁺ and Cl⁻ present), only hydrogen-bond acceptor property of chloride ions can be perceived. It suggests that the interaction of hydrated chloride ions with cellulose -OH groups could be weaker. The high acidic strength of HCl (i.e., low pKa value) can be supposed to control the gelation and neutralization of hydrated NaOH ions. It can assist to form rapidly a stable wet-gel network. As a result, the particles size appeared to be big in comparison to samples from weak organic acids.

This rapid self-association of cellulose fibers into a stable wet-gel network under strong acidic medium (H₂SO₄^[10b,i] and HNO₃^[10f]) were found in the literature. It was reported by Trygg et al.^[10f] that the strong acid, i.e., nitric acid can quickly form a stable gel network at the reaction front of a droplet forming wet-gel shell structure which preserves the shape and size of the beads.

When considering the beads size of Cell7-HCl as optimum particles size after acid-induced gelation, the decrease in the diameter of beads was 11.8%, 4.1% and 1.2% for aerogels produced from organic acids, i.e., Cell7-HCit, Cell7-HLac and Cell7-HAc respectively. It is due to the hydrogen-bond donor-acceptor behavior of the weak organic acids resulting the strong hydrogen-bond (van der Waal's) interaction to the surface of cellulose molecules in comparison to HCl.

Table 2. Size analysis from volume-based cumulative percentage curve Q3.

Sample	Mean diameter of beads, D_{50} (mm)		Particles size distribution, D_{90}/D_{10}	Diameter shrinkage/%	Volume shrinkage/%
	Initial ^[a]	Final ^[b]			
Cell7-HCl	3.83	3.25	1.0565	15.16	38.94
Cell7-HAc	3.78	3.28	1.1287	13.21	34.62
Cell7-HLac	3.67	3.15	1.1019	14.24	36.92
Cell7-HCit	3.37	2.88	1.1492	14.65	37.83

[a] The initial mean diameter of the wet-gel beads in the acid bath. [b] The final mean diameter of the beads after supercritical drying, i.e., aerogel beads.

The size distribution curve of the wet-gel beads is shown in Figure 2. The particles size distribution, (D_{90}/D_{10}) decreased in the following order: Cell7-HCIt, Cell7-HAc, Cell7-HLac and Cell7-HCl (see Table 2). Most narrow size particles were prepared from the Cell7-HCl. A broad particles size distribution was observed for Cell7-HAc. For the particles Cell7-HAc and Cell7-HCIt, the size distribution above D_{90} and below D_{10} , i.e., the volume of particles above 90% and below 10% was especially high in comparison to Cell7-HLac and Cell7-HCl. It revealed that maintaining the drop-height at certain distance (in the present case, 20 mm) for all the acid baths resulted in a broad particles size distribution for some acids.

Considering the real drop-height in the case of Cell7-HCl, the drop-height was calculated to be 20 mm, that agreed with the literature.^[109] For other samples, i.e., Cell7-HAc, Cell7-HLac

and Cell7-HCIt, the real drop-height was examined to be about 13, 40 and 70 mm, respectively. Because of this deviation from the set drop-height value (20 mm), the aerogel beads from those samples showed broad size distribution.

Table 3 shows the shape analysis data of the aerogel beads. The shape of the beads can be evaluated by sphericity and circularity values, and the data implies that the beads were highly spherical in shape. Span values supported the mono-disperse diameter distribution of the beads which were ≤ 0.1 for all samples and HCIt sample showed the largest value (0.1045). Span values and the particles size distribution showed the same trend. The values of cumulative coefficient of uniformity, C_u and the coefficient of curvature, C_c showed the packing property of the samples. As the samples were confirmed to be uniform in size and shape and the coefficients, C_u and C_c , showed values of about ~ 1 , the aerogel beads could be loosely packed with a high volume of interstitial air between the beads when they were randomly arranged.

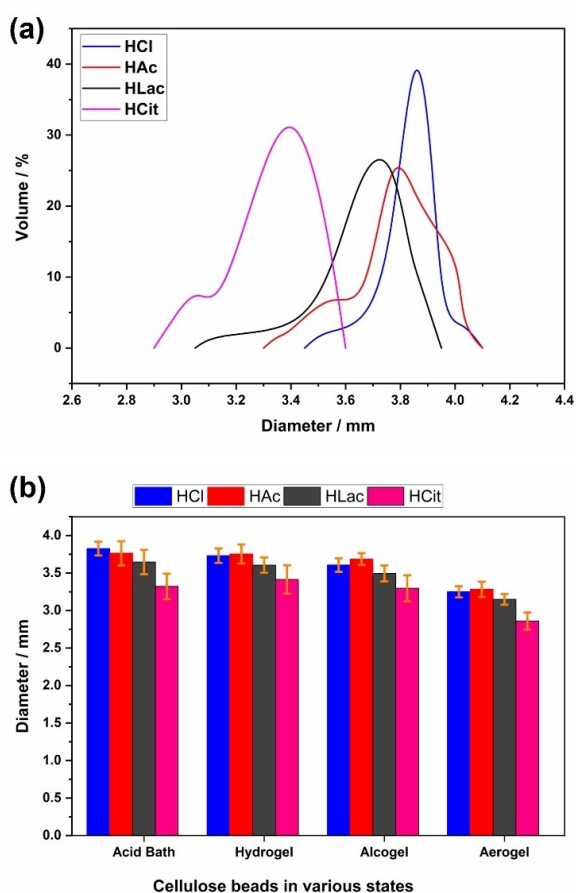


Figure 2. Illustrating particles size distribution of wet-gel beads in the acid bath (a), for reference see initial mean diameter values in Table 2, and the change in particles size in various stages (b).

Shrinkage Analysis of Beads

In comparison to the original particles size in the acid bath (see Table 2, Initial values), the mean diameter of the aerogel particles size changed while processing the aerogel, but no major deformation was observed.

The removal of the salts, additives and solvents by consecutive washing (H_2O), solvent exchange (ethanol) and $scCO_2$ drying induces shrinkage of the wet-gel body. Figure 2b shows the change in diameter of the beads in each step for all the samples. The change in diameter and the volume were calculated considering the high sphericity of the particles. The percentage of diameter shrinkage and volume shrinkage of aerogel beads are shown in Figure 3 and Table 2. The diameter shrinkage decreased in the following order of acids: HCl, HCIt, HLac and HAc. The total volume shrinkage of aerogel beads showed a trend similar to the diameter shrinkage after supercritical drying.

As per the literature,^[9a] the NaOH-water-based solvent medium can be comprised of a suspension of hydrated NaOH molecules in water independent of the presence of cellulose. Taking this into account, in the process of regeneration of cellulose using aqueous acidic bath, the reaction between the NaOH and the choice of acid play a vital role. Perceiving the rapid reaction between acid and base in aqueous medium, the act of promoting the hydrogen-bond interaction between the cellulose molecules, which can result in aggregation and gelation, can be influenced by the acid strength (pKa). Hence,

Table 3. Shape analysis of the aerogel beads from volume-based cumulative percentage curve Q3.

Sample	Sphericity	Circularity	Span	Cumulative coefficient of uniformity, C_u	Cumulative coefficient of curvature, C_c
Cell7-HCl	0.9965	0.9983	0.0609	1.0422	1.0044
Cell7-HAc	0.9965	0.9982	0.0793	1.0611	1.0043
Cell7-HLac	0.9966	0.9982	0.0608	1.0398	1.0021
Cell7-HCIt	0.9968	0.9984	0.1045	1.0808	1.0302

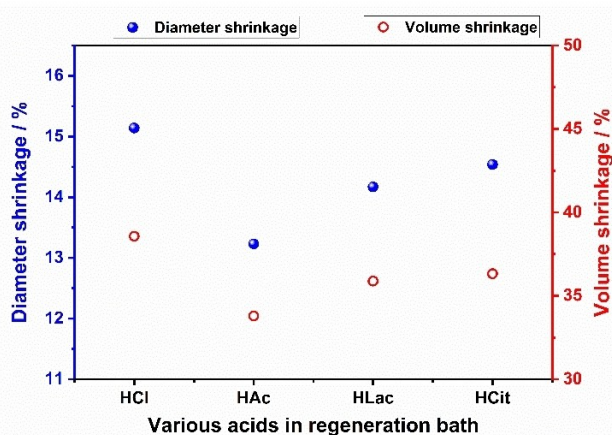


Figure 3. Total percentage of diameter shrinkage and volume shrinkage of cellulose beads after supercritical drying.

the stronger the acid can react with a strong base faster than a weak acid.

Thus, the strongest acid, HCl can induce a fast aggregation process of cellulose whereas the weakest acid, HAc can result in a slow process. Additionally, the monovalent anion formation can be faster in the following order of acid strength, i.e., HCl, HCit, HLaC and HAc according to the pKa values. The question may arise about HCit, which has three acidic carboxylic groups. In these experiments, considering the volume of acid and base, HCit in regeneration bath act as solvent and NaOH in cellulose droplet solution behave as solute. According to the literature,^[14] in reaction with NaOH, the monovalent anion of HCit can be predominantly formed instead of divalent or trivalent anion when the medium has a high concentration of HCit. As the concentration difference between solute (NaOH) and solvent (HCit) at the reaction front is high and fast ion exchange can happen in an aqueous medium, the regeneration of cellulose could have occurred only in the presence of HCit and the monovalent anion of HCit.

Considering the monovalent anion formation, the percentage of shrinkage showed a trend directly related to the strength of the acids (see Table 1). The strongest acid, HCl, having the lowest pKa value of acid in regeneration bath, may have caused the weakly interconnected network formation or loosely bound structures, which may result in a high percentage of volume shrinkage. Hence, the use of the weakest acid, i.e., HAc, with a high pKa value (4.76) provided the aerogel beads with the lowest volume shrinkage. As a result, the final aerogel beads size of HAc was bigger than HLaC and HCit.

For comparison, the volume shrinkage of xerogel was analyzed and it was observed to be about 92% in the case of Cell7-HAc.

Microstructure Analysis

Scanning electron microscope images of cellulose aerogel beads showed the microstructural differences after using

various acids in regeneration bath. For the microstructural analyses, it has to be considered that the cellulose aerogels are soft and ductile materials. Therefore, the artifacts should also be carefully taken care and there might be surface damage while preparing the samples. Figure 4 shows the topography of the exterior surface of cellulose aerogel beads. In general, for all the samples, an open porous network having meso- and macroporous structures was observed. The degree of distribution of meso- and macroporous structures varied between the samples. In the case of Cell7-HCl, there were loosely bound nanofibrillar network having large volume of macroporous networks whereas in the case of weak organic acids, the large volume of mesoporous structures was observed. In particular, the microstructure of Cell7-HCit exhibited the tightly packed nanofibrillar network and the mesoporous structure was finely distributed in comparison to the microstructure of Cell7-HCl sample. The impact of acids at the reaction front could have influenced the aggregation behavior of cellulose, leading to a stable shell layer on the surface of the droplet. Additionally, the continuous interaction of acids with the cellulose molecules induces shrinkage, reducing the pore volume between the cellulose nanostructures.

The inner microstructures of samples are shown in Figure 5. All samples were observed to have densely packed and randomly interconnected nanofibrillar networks of cellulose. In particular, comparing the images prepared from organic acids, Cell7-HCl samples showed very loosely bound interconnected nanofibrillar network because of the distribution of large volume of macroporous structure. In the case of organic acids, there were tightly bound nanofibrillar network and the finely distributed mesoporous structures were observed. It could be because of the slow acid-induced cellulose aggregation for the weak organic acids, especially in the interior of the beads. In brief, the strongest acid (HCl) generated loosely bound structure and large volume of macroporous structure. In order to confirm the vital role of acid strength in the production of macroporous structure, an indirect examination was carried out with the weakest acid (HAc) at various concentrations (from 0.5 to 4 M).

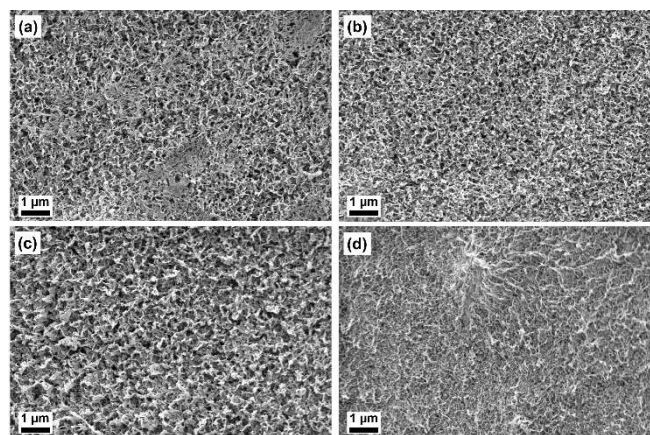


Figure 4. SEM images of the surface of cellulose aerogel beads gelled in different regeneration baths having 2 M concentration of acids: (a) HCl, (b) HAc, (c) HLaC and (d) HCit.

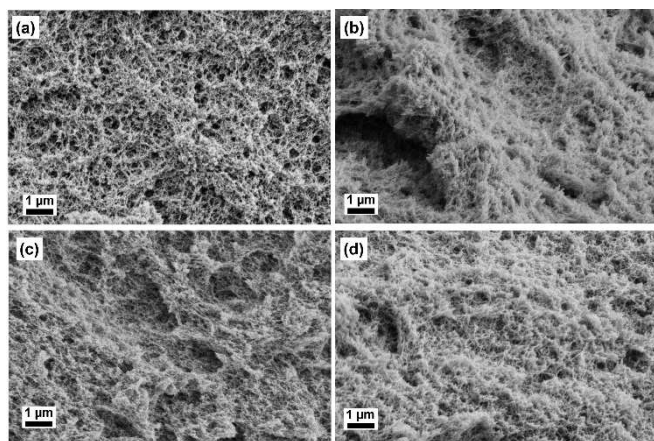


Figure 5. SEM images of the internal microstructures of cellulose aerogel beads gelled in different regeneration baths having 2 M concentration of acids: (a) HCl, (b) HAC, (c) HLac and (d) HCit.

Figure 6 shows the microstructures of Cell7-HAC samples at various concentrations of HAC. At the lowest concentration of HAC in the beads production (i.e., 0.5 M), the deformed beads

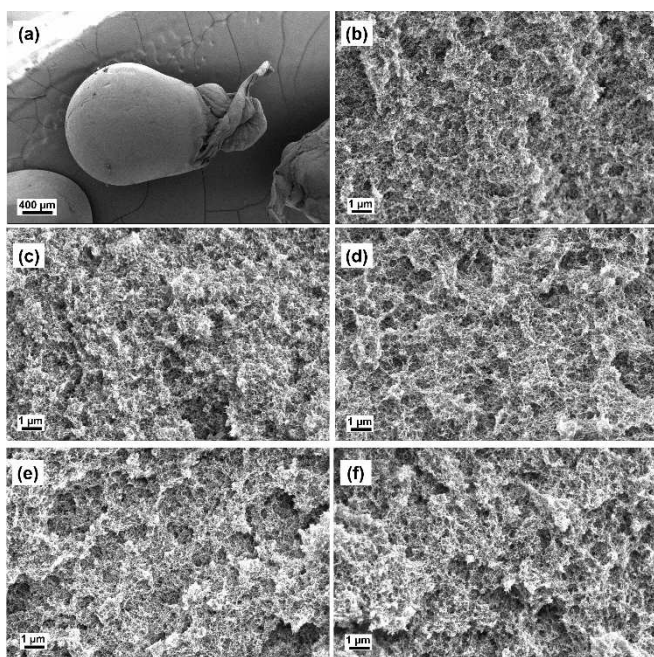


Figure 6. SEM images of cellulose aerogel beads prepared from 0.5 M of HAC in regeneration bath resulted in the shape deformation (a) and the internal microstructures of cellulose aerogel beads gelled in different concentration of aqueous HAC solution: (b) 0.5 M, (c) 1 M, (d) 2 M, (e) 3 M and (f) 4 M.

shape was observed (Figure 6a). However, the inner microstructure showed finely distributed nanofibrillar network and less macroporous structure. By increasing the acid concentration to 1, 2, 3 and 4 M, the nanofibrillar structure were still observed but the macroporous structures were increased. In the case of 4 M concentration (Figure 6f), due to the large volume of macroporous structure, the microstructure seemed to be agglomerated bundles of network but they composed of finely distributed nanofibrillar network. The results revealed that the macroporous structures can be generated by acid-induced gelation, specifically, by increasing the concentration of acid when acids with a high pKa value are employed or increasing the strength of acid (i.e., acids having low pKa) in the regeneration bath.

Physical Properties of Cellulose Aerogel Beads

a) Density and Porosity Analyses

The physical properties of cellulose aerogel beads (Cell7) obtained from 2M concentration of aqueous acidic regeneration bath are summarized in Table 4. The skeletal density is the density of the solid backbone of the material without considering the free pore space. For the commercial cellulose, the skeletal density was about 1.524 g cm^{-3} . No significant difference in skeletal density values was observed for different regenerated samples. Thus, the average skeletal density of cellulose aerogel beads of about 1.523 g cm^{-3} was taken as an input in Equation (7) for the calculation of the porosity of aerogels. This range of skeletal density values for regenerated cellulose (obtained from different solvent media) was observed in the literature.^[9c,15]

The envelope density of the aerogels was in the range between 0.18 and 0.23 g cm^{-3} . A low envelope density value for Cell7-HCl was observed in comparison to other samples. Referring to the discussion in the size and shape of the cellulose beads, the decrease in the size of initial wet-gel beads of Cell7-HCit (due to hydrogen-bond donor-acceptor behavior) and further shrinkage of the beads resulted in a high envelope density.

Equation (7) provided the porosity of aerogels which was in the range between 85% and 88%. It showed the same trend of envelope density, i.e., the bigger particles have a higher porosity than the smaller particles.

Table 4. Physical properties of cellulose aerogel beads (Cell7) obtained from 2 M concentration of aqueous acidic regeneration bath.

Sample	Envelope density/ g cm^{-3}	Porosity/%	BET Specific surface area/ $\text{m}^2 \text{g}^{-1}$	BJH pore volume/ $\text{cm}^3 \text{g}^{-1}$	Average pore size/nm
Cell7-HCl	0.18	88.2	387 ± 18	2.97	23.46
Cell7-HAc	0.21	86.2	423 ± 8	3.60	25.16
Cell7-HLac	0.21	86.2	402 ± 8	3.44	24.89
Cell7-HCit	0.23	84.9	397 ± 4	3.26	21.88

b) Specific Surface Area and Pore Structure Analyses

The porous structure and BET specific surface area of cellulose aerogel beads were obtained from nitrogen adsorption-desorption analyses (see Figure 7 and Table 4). Type IV isotherm was observed for all the samples (Figure 7a), as described by IUPAC.^[16] Each sample had different quantity of nitrogen sorption capacities during pore condensation in the relative pressure range between 0.7 and 1.0 (P/P^0). The aerogels produced from organic acids exhibited a significantly higher adsorption capacity in comparison with HCl. It indicated a difference in mesopore structure of various samples. Figure 7b displays a broad pore size distribution for all the samples. It must be perceived that BJH approximation is valid for mesopores (2–50 nm). For Cell7-HCl, the peak shifted to the low pore width range having an average pore size of 21.88 nm (see Table 4) and it seemed to be narrow having half height width of the peak between 17 and 35 nm. It can be due to the hydrogen-bond donor-acceptor behavior of HCl resulting tightly bound cellulose nano-network.

In the literature, where a similar dissolution method was used for the production of other cellulose aerogel beads and films,^[10d-f] the specific surface area values were reported in the range between 350 and 400 m^2g^{-1} . In the present study, Figures 7c and 7d show the BET specific surface area and BJH pore volume of Cell7-based aerogel beads at 2 M concentration of various acids, respectively. For Cell7-organic acids, the average BET specific surface area values were in the range

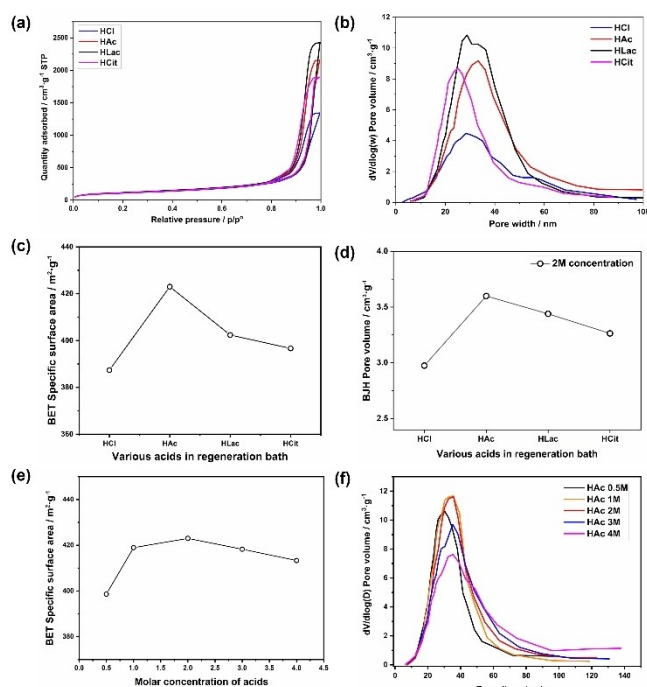


Figure 7. Nitrogen adsorption-desorption analysis of cellulose aerogel beads: (a) BET isotherm plot, (b) pore size distribution, (c) BET specific surface area and (d) BJH pore volume of Cell7-based aerogels prepared at 2 M concentration of various acids; (e) BET specific surface area and (f) BJH pore volume of Cell7-HAc samples at various molar concentrations of HAc. The data points are connected with line in order to guide the eye.

between 397 and 423 m^2g^{-1} . For Cell7-HCl, the average value was 387 m^2g^{-1} which was remarkably low (see Figure 7c). A similar trend was observed for the BJH pore volume (Figure 7d). Cell7-HCl sample showed low pore volume (2.97 cm^3g^{-1}) in comparison to Cell7-organic acids (3.26–3.6 cm^3g^{-1}).

Considering the SEM images in Figure 5, the comparison of the specific surface area and pore volume analysis data are in good agreement. Exhibiting the large macropores and loosely bound structure, Cell7-HCl showed low specific surface area and low pore volume in the mesopore range. Whereas, in the case of Cell7-organic acids, referring to the discussion in microstructure analysis, the weak organic acids-induced cellulose nano-network formation resulted in a high specific surface area, high pore volume in the mesopore range and the tightly bound nano-network of cellulose.

Further analysis was carried out in order to understand the influence of concentration of acids. Figures 7e and 7f show the average BET specific surface area and BJH pore volume for Cell7-HAc at various concentrations of HAc (from 0.5 to 4 M), respectively. At 0.5 M concentration of HAc, Cell7 exhibited very low specific surface area (about 399 m^2g^{-1}) in comparison to the concentrations ≥ 1 M where the specific surface area was in range between 413 and 423 m^2g^{-1} . The average pore volume was in the range between 3.1 and 3.6 cm^3g^{-1} . In specific, at 2 M concentration of HAc, it showed the highest specific surface area and the highest BJH pore volume. In Figure 7f, it was clearly observed that the increase in concentration of acid, ≥ 1 M of HAc, resulted in a broader pore size distribution indicating the existence of less mesoporous structure. Meanwhile, at the lowest concentration of acid, i.e., for 0.5 M of HAc, it was noticed a narrow pore size distribution in the mesopore range. It appears that the increase in acid concentration in the regeneration bath resulted in forcing the cellulose nano-structures to rapidly aggregate with fewer mesoporous structures and an increase in macropores. This pore size distribution data agrees with the SEM images of Cell7-HAc in Figure 6.

Analysis of Cell5, Cell6 and Cell7-based aerogel beads prepared at 2 M concentration of HAc showed no major change in the average BET specific surface area values. It implies that the increase in cellulose concentration resulted in the same fiber thickness because of the same tendency of aggregation at constant regeneration bath (2 M), which agrees with the literature.^[10i]

Crystallinity Analyses

Figure 8 shows the powder X-ray diffraction (XRD) pattern of cellulose aerogel beads after regeneration in HAc as an example representing the regenerated cellulose. The first noticeable aspect of the XRD pattern was that the peaks of Cell7-HAc were broader than the peaks detected for commercial cellulose which was employed in the synthesis of cellulose aerogel beads. Besides, the peak shifts were detected for Cell7-HAc aerogels in comparison with the reference commercial sample. The intense diffraction peak from native commercial cellulose was shifted from 22.6° to 20.5° as a broad peak after dissolution

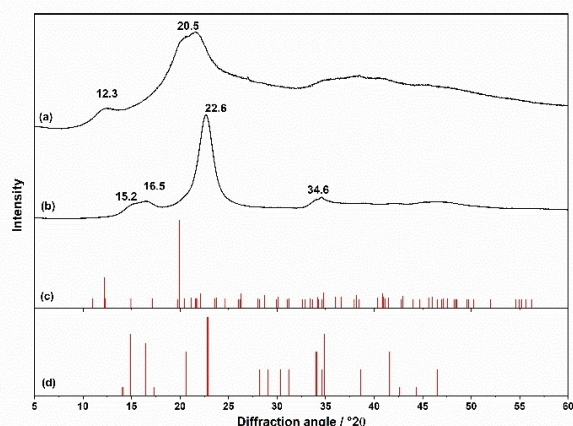


Figure 8. Powder X-ray diffraction pattern showing the change in crystallinity of cellulose after regeneration in HAC bath (a) and commercial cellulose (b); (c) and (d) are the reference diffraction patterns of cellulose II (PDF number = 00-056-1717) and native cellulose I (PDF number = 00-003-0289), respectively, which are obtained from the International Center for Diffraction Data.

and regeneration. In comparison with the reference diffraction patterns of cellulose II and native cellulose I (Figure 8c and d), it can be determined that the regenerated cellulose can have a mixture of cellulose II and amorphous cellulose. During the dissolution process of commercial cellulose and the regeneration of beads, the alignment of the cellulose chain can be changed from parallel to antiparallel orientation.^[17] As a result, the change in crystallinity occurred.

FTIR Spectral Analyses

FTIR spectral analyses were carried out for all cellulose aerogel beads (Figure 9). For reference, the data was compared with

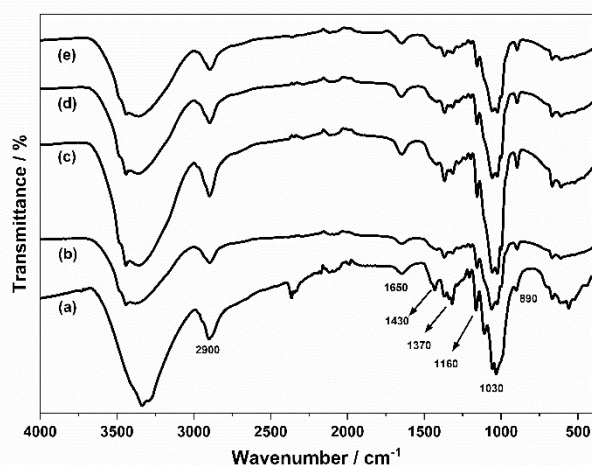


Figure 9. Comparison of FTIR spectra of commercial cellulose (a) which was used as starting material in the aerogels synthesis and cellulose aerogel beads: Cell7-HCl (b); Cell7-HAC (c); Cell7-HLac (d); Cell7-HCit (e).

commercial cellulose (Figure 9a). The vibrational bands at 3300 cm^{-1} and 2900 cm^{-1} were assigned to the $-\text{OH}$ and $-\text{CH}$ stretching vibrations, respectively. The adsorbed water molecules showed a small band at 1650 cm^{-1} . The vibrational band at 1430 cm^{-1} was assigned to the $-\text{CH}_2$ bending which can be used as a characteristic band for analyzing the crystalline polymorphs of cellulose (cellulose I or cellulose II). For cellulose II, this vibrational band became broader between 1419 and 1460 cm^{-1} which was observed in all the aerogel beads. The vibrational bands at 1160 cm^{-1} and 1030 cm^{-1} were assigned to $\text{C}-\text{O}-\text{C}$ asymmetric stretching and ring asymmetric stretching of $\text{C}-\text{O}$, respectively. The spectra for all the cellulose aerogel beads were extremely similar, indicating no impurities and showing the vibrational bands of pure regenerated cellulose.

Conclusion

Various acids were examined as regeneration media for the production of cellulose aerogel beads. All acids in common yielded a high quality regenerated cellulose aerogel beads having cellulose II structure and no impurities. The weak organic acids showed significant impact on tailoring the physical properties of cellulose aerogel beads. The carboxylic acid functional group in weak acids, which has a high hydrogen-bond donor-acceptor property, played a vital role in determining the shrinkage behavior, specific surface area, pore volume and microstructure. The weakest acid, HAC, can be a good choice to produce cellulose aerogel beads with less shrinkage, high pore volume and high specific surface area. A strong acid, HCl, or a high concentration of weak acid can be used to improve the macroporous structure. In demand, the other organic or inorganic acids can also be used to produce cellulose aerogels for the specific application if certain properties such as macroporous structure or narrow pore size distribution are required.

Experimental Section

Materials

Sodium hydroxide (NaOH, ACS grade, VWR), cellulose medium fibers (product number: C6288, Sigma-Aldrich), urea (Sigma-Aldrich), hydrochloric acid (37%, Panreac-AppliChem), glacial acetic acid (pure, Panreac-AppliChem), anhydrous citric acid (Merck) and lactic acid (90% in water, Bernd Kraft) were purchased and used without further purification. Deionized water was used for all the experiments. Ethanol (99%) having 1% of methyl ethyl ketone or petroleum ether was used for solvent exchange process. The CO_2 gas bottles for supercritical drying were supplied by Air Liquid.

Characterization Techniques

The following analytical techniques were used to characterize the structural and physical properties of the aerogel beads. The skeleton and the envelope densities were determined by Micromeritics - Accupyc II 1340 (helium gas) and Micromeritics - Geopyc 1360 (25 N, using a dry-flow medium), respectively. Nitrogen

sorption measurements were performed using Micromeritics – Tristar II 3020 instrument. Brunauer–Emmett–Teller (BET) and Barrett–Joyner–Halendar (BJH) analyses were done using the Micro-Active (v5.02) software. The BET analysis was carried out for a relative pressure (P/P^0) range between 0.05 and 0.3 at 77 K. BJH analysis was performed from the desorption curve of the isotherm. Fourier transform infrared (FTIR) spectra, ATR mode, were recorded in the region of 400–4000 cm^{-1} using a Bruker-Tensor 27 instrument at a resolution of 4 cm^{-1} . For morphology study, images were captured by scanning electron microscopy using a Zeiss - Ultra 55 with Gemini column (operated at 2–6 kV). All samples were coated with platinum, for 90 sec, at 0.04 mbar and 21 mA, using the sputtering system SCD 500 from BALTEC, as pre-treatment. Krüss Force Tensiometer K100 was used for the analyses of the liquid densities (Archimedean principle) and the surface tension (Du Noüy ring method) of the aqueous acidic solutions (2 M) at 23 °C. A Zeiss Axiocam 208 color optical microscope was used for morphology and dimension analysis. The XRD measurements were carried out on a Bruker D8 ADVANCE A25 diffractometer using Cu-K α radiation ($\lambda = 1.54 \text{ \AA}$). The XRD spectra were recorded from 5° to 80° (2 θ) at a scan rate of 3°/min. The standard parameter for the single crystal reflection mode was 35 kV and 30 mA. Thermogravimetric analyses were performed using a NETZSCH STA 449F3 thermal analyzer. Samples were processed in an Al₂O₃ open crucible and heated up to 600 °C at a rate of 5 K/minute, under argon atmosphere. The viscosity of Cell7 solution was analyzed at the Rheometer Haake Mars 60 from ThermoFisher Scientific. The viscosity of Cell7 was 0.3 Pa·s at a shear rate of 1000 s^{-1} .

Shrinkage

In the present study, the particles were considered to be perfect spheres as they were produced using syringe dropping technique. The diameter and the volume of the wet-gel beads obtained from aqueous acidic medium were set as D_0 and V_0 , respectively. The percentage of shrinkage was calculated from them. For statistic reasons, the average diameter for each sample was measured by analyzing at least 25 beads. The total percentage of diameter shrinkage of the sample was measured by following Equation (1)^[18] where D_1 is an average diameter of the aerogel after supercritical drying. For volume shrinkage, the changes occurred in each step were analysed using Equation (2). The value of V_1 can be the volume of alcogel, aerogel or xerogel.

$$\text{Diameter shrinkage (\%)} = \frac{(D_0 - D_1)}{D_0} \times 100 \quad (1)$$

$$\text{Volume shrinkage (\%)} = \frac{(V_0 - V_1)}{V_0} \times 100 \quad (2)$$

Sphericity

Sphericity, ψ , of the aerogel particles was calculated from the ratio of the surface area of an equal volume of a sphere to the actual surface area of the particle (see Equation (3)^[19]). Here, V_{aerogel} is the volume of the aerogel particles and A_{aerogel} is the area of aerogel particles. The sphericity of an ideal spherical sample must be the value equal to 1 whereas it is < 1 for the non-spherical particle. Circularity can be calculated from sphericity, i.e., the square root of sphericity.

$$\psi = \frac{\pi^{1/3} (6V_{\text{aerogel}})^{2/3}}{A_{\text{aerogel}}} \quad (3)$$

Volume-Based Size Distribution of Cumulative Curve

Mean diameter of the beads, D_{90} , D_{60} , D_{50} , D_{30} and D_{10} were obtained from the volume-based size distribution against the cumulative percentage curve (Q_3) at 90%, 60%, 50%, 30% and 10%, respectively. The span of volume-based particles size distribution was calculated using Equation (4) and it showed the diameter distribution of particles when different acids were employed in the regeneration bath.

$$\text{Span} = \frac{(D_{90} - D_{10})}{D_{50}} \quad (4)$$

Cumulative uniformity coefficient (C_u) and coefficient of degradation (C_c) were calculated from Equations (5 and 6), respectively.

$$C_u = \frac{D_{60}}{D_{10}} \quad (5)$$

$$C_c = \frac{D_{30}^2}{D_{10} \cdot D_{60}} \quad (6)$$

Porosity

The porosity of the beads was calculated by applying their respective envelope (ρ_e) and the average skeletal density (ρ_s) in Equation (7).^[20]

$$\text{Porosity in \%} = \left(1 - \frac{\rho_e}{\rho_s} \right) \times 100 \quad (7)$$

Preparation of Cellulose Aerogel Beads

7 g of sodium hydroxide was dissolved in distilled water (81 g). After cooling to room temperature, cellulose fibers (for example, 7 g of cellulose for Cell7 sample) were added to the sodium hydroxide solution. The suspension was stirred for about 10 minutes, promoting the swelling of the cellulose. Then the mixture was cooled in an ice bath to 0 °C and stirred for one hour. Afterwards, 12 g of urea was added to this mixture and stirring continued for one more hour. The dissolution of urea is an endothermic reaction. Then it was left stirring at room temperature. The mixture was observed to be clear liquid. Subsequently, it was stored at –20 °C for 18 hours. For further processing, the mixture was brought to room temperature. It appeared to be pale yellow clear viscous liquid. The solution was stirred for a while in order to make it homogeneous. The solution was then sonicated for 15 minutes to remove any bubbles and transferred to a plastic container which was equipped with nozzle tips (the inner diameter of a nozzle is about 1 mm). The cellulose solution fell in the form of droplets to a regeneration bath containing 2 M aqueous acidic solution. The regeneration bath was gently stirred to keep the solution homogeneous. The drop height was of 20 mm and the

droplets gelled into beads, creating white spheres. After gelation, the beads were washed five to seven times with deionized water in order to remove salts and excess acidic medium. In each washing step, after 30 minutes of stirring, the pH of the supernatant liquid was controlled. After neutralization, a five step-wise solvent exchange process was carried out by gradually increasing the ethanol concentration (in each step, increase of 20 vol%) in a water-ethanol mixture. The final ethanol containing beads were washed two more times with ethanol in order to remove any trace amount of water. The samples were dried in an autoclave (60 L), for 9 hours using supercritical carbon dioxide (scCO₂), at 11.5 MPa between 25 °C and 60 °C.

Various amount of cellulose in NaOH-urea-water mixture was examined for the preparation of cellulose beads. The weight ratio of cellulose fibers to NaOH-urea-water mixture was maintained as 5, 6 or 7 g of cellulose to 100 g of NaOH-urea-water mixture and the samples were named as Cell5, Cell6 and Cell7, respectively.

Acknowledgements

This project has received funding from the European Union's Horizon 2020 research and innovation programme under Marie Skłodowska-Curie grant agreement ID: 956621. We gratefully thank Mrs. Rebekka Probst for her help in imaging the scanning electron microscope pictures. We thank Mr. Temple Nwakanma for his experimental data support while working on his Master's thesis. We thank Mr. Alexander Francke for his assistance with Powder X-Ray diffraction data. Open Access funding enabled and organized by Projekt DEAL.

Conflict of Interest

The authors declare no conflict of interest.

Keywords: Aerogel · Cellulose beads · Carboxylic acid · Porous structure · Regeneration bath

- [1] a) S. S. Kistler, *J. Phys. Chem* **1932**, *36*, 52–64; b) S. S. Kistler, *Nature* **1931**, *127*, 741.
- [2] a) R. Mavelil-Sam, L. A. Pothen, S. Thomas, in *Biobased Aerogels: Polysaccharide and Protein-based Materials* (Eds.: S. Thomas, L. A. Pothen, R. Mavelil-Sam), The Royal Society of Chemistry, London, **2018**, pp. 1–8; b) L. E. Nita, A. Ghilan, A. G. Rusu, I. Neamtu, A. P. Chiriac, *Pharmaceutics* **2020**, *12*, 449; c) S. Zhao, W. J. Malfait, N. Guerrero-Alburquerque, M. M. Koebel, G. Nystrom, *Angew. Chem. Int. Ed.* **2018**, *57*, 7580–7608.
- [3] Y. Han, X. Zhang, X. Wu, C. Lu, *ACS Sustain. Chem. Eng.* **2015**, *3*, 1853–1859.
- [4] S. T. Nguyen, J. Feng, S. K. Ng, J. P. W. Wong, V. B. C. Tan, H. M. Duong, *Colloids Surf. A* **2014**, *445*, 128–134.
- [5] Z. Saadatnia, S. Ghaffari Mosanenzadeh, M. Marquez Chin, H. E. Naguib, M. R. Popovic, *IEEE Trans. Biomed. Eng.* **2021**, *68*, 1820–1827.
- [6] a) O. Payanda Konuk, A. A. M. Alsuhile, H. Yousefzadeh, Z. Ulker, S. E. Bozbag, C. A. García-González, I. Smirnova, C. Erkey, *Front. Chem.* **2023**, *11*, 1294520; b) L.-Y. Long, Y.-X. Weng, Y.-Z. Wang, *Polymers* **2018**, *10*, 623; c) K. Ganesan, T. Budtova, L. Ratke, P. Gurikov, V. Baudron, I. Preibisch, P. Niemeyer, I. Smirnova, B. Milow, *Materials* **2018**, *11*, 2144.
- [7] a) P. Gurikov, R. S. P. J. S. Griffin, S. A. Steiner, I. Smirnova, *Ind. Eng. Chem. Res.* **2019**, *58*, 18590–18600; b) R. Subrahmanyam, P. Gurikov, P. Dieringer, M. Sun, I. Smirnova, *Gels* **2015**, *1*, 291–313; c) N. Buchtová, T. Budtova, *Cellulose* **2016**, *23*, 2585–2595; d) J. Qiu, X. Guo, W. Lei, R. Ding, Y. Zhang, H. Yang, *Nanomaterials* **2023**, *13*, 613.
- [8] a) T. Budtova, *Cellulose* **2019**, *26*, 81–121; b) F. Liebner, E. Haimer, A. Potthast, T. Rosenau, in *Polysaccharide building blocks: a sustainable approach to the development of renewable biomaterials*, First ed. (Eds: Y. Habibi, L. A. Lucia), John Wiley & Sons, Inc., New Jersey, **2012**.
- [9] a) R. Gavillon, T. Budtova, *Biomacromolecules* **2007**, *8*, 424–432; b) R. Sescousse, R. Gavillon, T. Budtova, *Carbohydr. Polym.* **2011**, *83*, 1766–1774; c) N. Pircher, L. Carbajal, C. Schimper, M. Bacher, H. Rennerhofer, J.-M. Nedelec, H. C. Lichtenegger, T. Rosenau, F. Liebner, *Cellulose* **2016**, *23*, 1949–1966.
- [10] a) S. Ookuma, K. Igarashi, M. Hara, K. Aso, H. Yoshidome, H. Nakayama, K. Suzuki, K. Nakajima, Vol. *US5196527A* (Ed.: K. Ltd), Kanebo Ltd., Tokyo, Japan, Japan, **1988**; b) L. Zhang, Y. Mao, J. Zhou, J. Cai, *Ind. Eng. Chem. Res.* **2005**, *44*, 522–529; c) R. Gavillon, Ph.D. thesis, École Nationale Supérieure des Mines de Paris (France), **2007**; d) J. Cai, S. Kimura, M. Wada, S. Kuga, L. Zhang, *ChemSusChem* **2008**, *1*, 149–154; e) N. Isobe, U. J. Kim, S. Kimura, M. Wada, S. Kuga, *J. Colloid Interface Sci.* **2011**, *359*, 194–201; f) J. Trygg, P. Fardim, M. Gericke, E. Mäkilä, J. Salonen, *Carbohydr. Polym.* **2013**, *93*, 291–299; g) S. M. Kamal Mohamed, K. Ganesan, B. Milow, L. Ratke, *RSC Adv.* **2015**, *5*, 90193–90201; h) P. Parajuli, S. Acharya, Y. Hu, N. Abidi, *J. Appl. Polym. Sci.* **2020**, *137*, 48975; i) B. Schroeter, V. P. Yonkova, N. A. M. Niemeyer, I. Jung, I. Preibisch, P. Gurikov, I. Smirnova, *Cellulose* **2021**, *28*, 223–239.
- [11] R. Sescousse, T. Budtova, *Cellulose* **2009**, *16*, 417–426.
- [12] A. Albert, E. P. Serjeant, *The Determination of Ionization Constants: A Laboratory Manual*, 3 ed., Springer Dordrecht, The Netherlands, **1984**, 218.
- [13] E.-S. Chan, B.-B. Lee, P. Ravindra, D. Poncelet, *J. Colloid Interface Sci.* **2009**, *338*, 63–72.
- [14] A. Apelblat, *Citric Acid*, 1 ed., Springer Cham, **2014**, 357.
- [15] K. Ganesan, A. Dennstedt, A. Barowski, L. Ratke, *Mater. Design* **2016**, *92*, 345–355.
- [16] M. Thommes, K. Kaneko, A. V. Neimark, J. P. Olivier, F. Rodriguez-Reinoso, J. Rouquerol, K. S. W. Sing, *Pure Appl. Chem.* **2015**, *87*, 1051–1069.
- [17] P. Zugenmaier, *Crystalline Cellulose and Cellulose Derivatives*, Springer-Verlag Berlin Heidelberg, Heidelberg, Germany **2008**, 285.
- [18] T. Zhang, Y. Zhang, H. Jiang, X. Wang, *Mater. Res. Express* **2019**, *6*, 075027.
- [19] H. Wadell, *J. Geol.* **1935**, *43*, 250–280.
- [20] S. Beluns, S. Gaidukovs, O. Platnieks, G. Gaidukova, I. Mierina, L. Grase, O. Starkova, P. Brazdauskis, V. K. Thakur, *Ind. Crop. Prod.* **2021**, *170*, 113780.

Manuscript received: May 7, 2024

Accepted manuscript online: June 30, 2024

Version of record online: August 14, 2024